Glycomimetics

Conformational Plasticity in Glycomimetics: Fluorocarbamethyl-L-idopyranosides Mimic the Intrinsic Dynamic Behaviour of Natural Idose Rings

Luca Unione,[a, c] Bixue Xu,[b, g] Dolores Díaz,[a] Sonsoles Martín-Santamaría,[a] Ana Poveda,[c] João Sardinha,[b, e] Amelia Pilar Rauter,[e] Yves Blériot,[f] Yongmin Zhang,[b] F. Javier Cañada,[a] Matthieu Sollogoub,*[b] and Jesus Jiménez-Barbero*[a, c, d]

Abstract: Sugar function, structure and dynamics are intricately correlated. Ring flexibility is intrinsically related to biological activity; actually plasticity in L-iduronic rings modulates their interactions with biological receptors. However, the access to the experimental values of the energy barriers and free-energy difference for conformer interconversion in water solution has been elusive. Here, a new generation of fluorine-containing glycomimetics is presented. We have applied a combination of organic synthesis, NMR spectroscopy and computational methods to investigate the conformational behaviour of idose- and glucose-like rings. We have used low-temperature NMR spectroscopic experiments to slow down the conformational exchange of the idose-like rings. Under these conditions, the exchange rate becomes slow in the ^{19}F NMR spectroscopic chemical shift timescale and allows shedding light on the thermodynamic and kinetic features of the equilibrium. Despite the minimal structural differences between these compounds, a remarkable difference in their dynamic behaviour indeed occurs. The importance of introducing fluorine atoms in these sugars mimics is also highlighted. Only the use of ^{19}F NMR spectroscopic experiments has permitted the unveiling of key features of the conformational equilibrium that would have otherwise remained unobserved.

[a] L. Unione,+ Dr. D. Díaz, Dr. S. Martín-Santamaría, Prof. F. J. Cañada, Prof. J. Jiménez-Barbero
Chemical and Physical Biology Department
Centro de Investigaciones Biológicas, CIB-CSIC
Ramiro de Maeztu 9, 28040 Madrid (Spain)
E-mail: jjbarbero@cicbiogune.es

[b] Dr. B. Xu,+ Dr. J. Sardinha, Y. Zhang, Prof. M. Sollogoub
Sorbonne Universités, UPMC Univ Paris 06, Institut Universitaire de France
UMR CNRS 8232, IPCM, 4, place Jussieu, 75005 Paris (France)
E-mail: matthieu.sollogoub@upmc.fr

[c] L. Unione,+ Dr. A. Poveda, Prof. J. Jiménez-Barbero
Infectious Disease Programme, CIC bioGUNE, 48160 Derio, Bizkaia (Spain)

[d] Prof. J. Jiménez-Barbero
IKERBASQUE, Basque Foundation for Science, 48011 Bilbao (Spain)

[e] Dr. J. Sardinha, Prof. A. P. Rauter
Centro de Química e Bioquímica
Faculdade de Ciências da Universidade de Lisboa, Edifício C8
1749-016 Lisboa (Portugal)

[f] Prof. Y. Blériot
Université de Poitiers, UMR CNRS 7285, IC2MP, Equipe Synthèse organique, Groupe Glycochimie, 4, avenue Michel Brunet, 86022 Poitiers Cedex (France)

[g] Dr. B. Xu+
Present address: The Key Laboratory of Chemistry for Natural Products of Guizhou Province and Chinese Academy of Sciences
202 Shachong South Road, Guiyang, 550002 (P.R. China)

[+] These authors contributed equally to this work.

Supporting information for this article is available on the WWW under http://dx.doi.org/10.1002/chem.201501249. It contains eighteen figures and five tables including NMR spectra of the discussed compounds, NOEs and J coupling analysis of the experimental data, structures, synthesis and computational data.

Introduction

The specific interaction between sugars and their natural receptors (e.g., lectins) is responsible for triggering many crucial biological processes, cells–cell and cell–host dialogues, immune response, etc.[1, 2] Thus, from a biomedical viewpoint, the knowledge about both the chemical and structural factors that are decisive for establishing effective interactions are of great interest for the development of new potential glycan-based drugs.[3] Hence, the field of glycosciences has experienced in the last years a blossom in research to reveal the structure–activity relationships (SARs) that govern the effectiveness of carbohydrate–protein interactions.[4, 5] Thus, biophysical techniques, such as X-ray crystallography or NMR spectroscopy,[6] among others, usually assisted by molecular modelling, have been successfully employed to assess the structural, dynamic, and conformational requirements that favour the formation of sugar–protein complexes.[7, 8] However, natural sugars are subject to degradation processes under natural conditions in tissues and biofluids and therefore, a variety of chemical analogues have been designed and synthesized to overcome this problem. Thus, different glycomimetics have been reported that compete with their natural counterparts for the same receptors or enzymes acting, consequently, as molecular probes or enzyme inhibitors.[9] Generally speaking, two major groups of sugar mimics have been devised by substitution of either the *endo-* or *exo-*cyclic oxygen atom by an-

other atom (e.g. carbon, sulfur, nitrogen).[10,11] However, their conformational preferences, as well as their internal hydrogen-bond patterns, might differ from their natural analogues in a way that could also influence their interactions with the key residues within the binding site of sugar receptors.[12] For instance, for carbasugars, for which the ring oxygen has been replaced by a methylene group,[13] this substitution rules out the anomeric effects, modifies the intramolecular hydrogen-bond pattern, modulates the amphiphilicity of the sugar ring, and results in changes in the flexibility and conformations population distributions.[14]

Figure 1. Sugar ring conformations of the α-IdoA unit. Structural representation of the sugar ring conformations (chairs, C, and skew-boat, S) of the α-IdoA unit, observed in glycosaminoglycans, such as heparin and heparan sulfate. Carbon atoms are numbered according to their positions within the sugar ring.

Fluorine is not an endogenous nucleus, but medicinal chemistry studies have demonstrated its useful introduction in bioactive substances to improve their pharmacokinetics properties and to modulate its biological properties. From the NMR perspective, the presence of ^{19}F atoms may also deliver important conformational and structural information, complementary to that provided by ^{1}H and ^{13}C nuclei.[15]

For all these reasons, fluorinated glycomimetics have received careful attention.[16] Depending on the substituted position, the fluorine substituent can have a remarkable effect upon the physical and chemical properties of the molecule. It could induce increase of lipophilicity, decrease in pK_a values of certain groups by OH–F electrostatic interaction, modulate the hydrogen-bond acceptor/donator ability or foster the presence of a particular ring conformation.[17]

In this context, difluorinated carbasugars have been recently synthesized.[18–20] Their suitability to act as improved sugar analogues has been studied. Indeed, the presence of fluorine atoms emulates, to a certain degree, the properties of the endocyclic oxygen[20] and, consequently, they are better candidates to mimic natural glycans than their non-fluorinated analogues. The possibility of the presence of intramolecular OH–F hydrogen bonds should also be explored, along with their structural and conformational implications.[21] In principle, in those cases for which the bound conformation resembles the ground state of the natural saccharide, glycomimetics with closer conformational behaviour would be desirable. One of the paradigmatic cases of conformational dynamics in glycosciences is that of the Iduronic acid (L-IdoA) moiety present in heparin. The extent of conformational mobility of L-IdoA in heparin oligosaccharides in both the free and bound states has also been matter of debate,[22] especially focused on the $^{4}C_1$-chair–skew boat-$^{1}C_4$ chair equilibrium of the pyranose rings in the free and protein-bound states (Figure 1). Interestingly, depending on the protein receptor, distinct conformations of the L-IdoA ring are recognized.[23] Indeed, AT-III recognizes the skew boat conformer,[24] while the IdoA rings of a heparin hexasaccharide maintain the chair–skew boat flexibility when bound to FGF-1.[25] Fittingly, for AT-III case, Sinaÿ et al. prepared skew-boat conformationally locked compounds that keep the
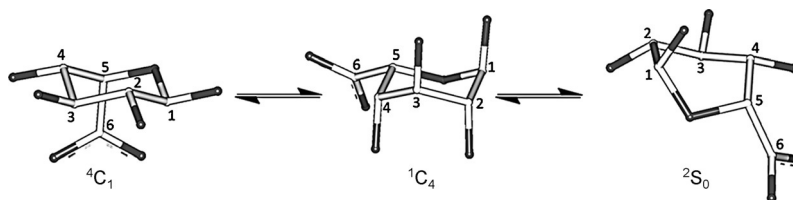
biological activity, thus providing direct evidence on the recognition of these conformers by AT-III.[26] Obviously, this dynamic behaviour has key implications in the kinetics and thermodynamics of the molecular recognition event. Nevertheless, the access to idose mimics that retain conformational plasticity and the quantification of the experimental values of the energy barriers and free-energy differences for the chair–skew boat interconversion processes in water solution has remained elusive. Recent efforts using O-substituted Ido compounds have provided energy values in organic solvents.[27,28] However, given the intrinsic relative low energy barrier for this equilibrium, NMR spectroscopic experiments in water using hydroxylated natural compounds have failed to slow down the equilibrium to provide quantitative and non-ambiguous values.

On this basis, we herein present the synthesis and conformational analysis of different fluorine-containing Ido-mimetics. Thus, we have investigated two *gem*-difluorocarbasugars **1a** and **2** both analogues to methyl-β-L-idopyranoside and possessing either a quaternary or a ternary C5 respectively. As a model compound, we have also studied the corresponding Glc analogue **1b** (Figure 2), since Glc pyranose rings are usually
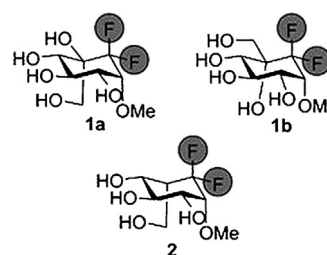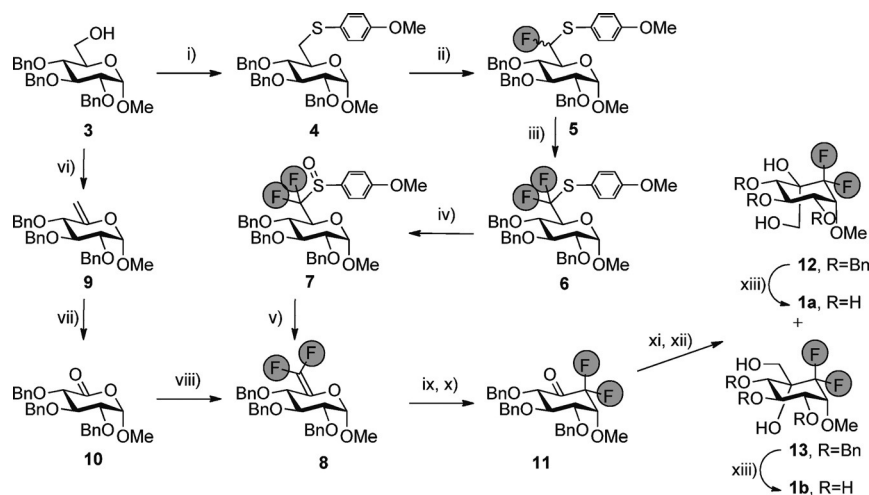

Figure 2. Schematic representation of glycomimetics discussed in this work.

conformationally stable. ^{19}F and ^{1}H homo- and heteronuclear NMR spectroscopic methods have been applied in water and dimethyl sulfoxide solutions to determine their intrinsic conformational and structural properties. The experimental NMR spectroscopic data have been supported by computational methods to unambiguously unravel the structural and conformational effects of the difluoromethylene function.

Synthesis of compounds **1a** and **1b** used a similar route to the one we designed to make *gem*-difluorocarbadisaccharides,[20] and involved a Pummerer reaction to make the difluorinated *exo*-glycal.[29] Sulfidation of alcohol **3**[30] was achieved by

treatment with bis(4-methoxyphenyl) disulfide and tributyl-phosphine in DMF to afford sulfide **4** in 96% yield. Fluorination of sulfide **4** was performed using a Pummerer reaction, sulfide was first oxidized to the sulfoxides using *m*-chloroperbenzoic acid (*m*CPBA), then treatment with (diethylamino)sulfur trifluoride (DAST) gave monofluorosulfides **5** in 96% yield as a mixture of two inseparable diastereomers. The second fluorination was realized through reaction of **5** with Selectfluor in the presence of DAST, followed by the addition of diisopropylethylamine (DIPEA) to afford desired difluorosulfide **6** in 60% yield. Another *m*CPBA oxidation of the difluorosulfide **6** gave sulfoxides **7** in 77% yield as an inseparable mixture of diastereomers. Thermolysis of difluorosulfoxides **7** was achieved using Bn_3N in Ph_2O at 190 °C under air for 120 h to give the difluoroalkene **8** in 36% yield. An alternative route to alkene **8** was also explored starting from known alkene **9** synthesized from **3**. Hexoglucal **9**[31] was converted into lactone **10** by ozonolysis,[32] and **10** was converted into **8** using a Wittig olefination. However, this last step appeared to be rather delicate to implement. Treatment of the difluorovinyl compound **8** with triisobutylaluminium (TIBAL) gave the desired carbacycle,[33–37] which was oxidized into ketone **11** with Dess–Martin periodinane. Reaction of freshly prepared Tamao's reagent on **11** provided β-hydroxysilanes, which were subjected, without purification, to oxidative cleavage of the Si–C bond by basic hydrogen peroxide to give diols **12** and **13**, which were separated. Final deprotections of both **12** and **13** through hydrogenolysis using Pd/C gave the target *gem*-difluorocarbasugars **1a** and **1b** in quantitative yields. (Scheme 1; for synthesis of compound **2**, see the Supporting Information).

Results and Discussion

NMR spectroscopy

Compounds **1a** and **1b** only differ in the configuration of the stereogenic center at C5 (Figure 2). Strikingly, the observed ^1H, and especially the ^{19}F NMR spectra for both molecules, were dramatically different (Figure 3). The assignment of the two ^{19}F
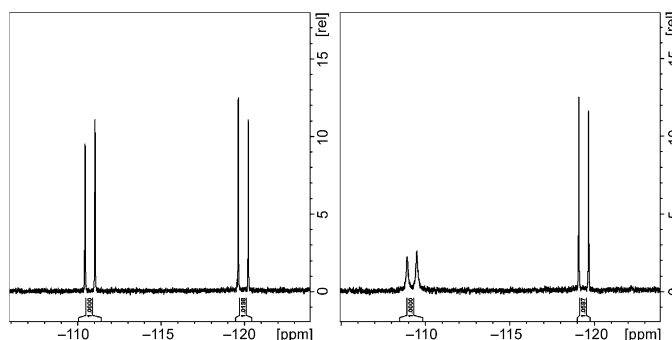

Figure 3. ^{19}F NMR (470 MHz) spectra of **1b** (left) and **1a** (right) in the solvent D_2O. Notice the broad shape of the axial fluorine resonance signal of **1a**. The integrals (1:1) are also shown.

resonances allowed us to determine that the broad signal observed in **1a** corresponds to the axially oriented fluorine atom. As deduced from the visual inspection of the shape of the equatorial fluorine in **1a**, as well as of those of both fluorine atoms in **1b**, the behaviour of the axial fluorine of **1a** was rather unique. Given this particular feature, a detailed conformational analysis by using NMR spectroscopic methods was then performed. Tables 1 and 2 gather the chemical shift and *J*-coupling data for the three study molecules compared to the data for natural methyl-L-idopyranoside[38] and methyl-D-glucopyranoside[39] used as reference compounds. The observations for the different molecules are given below:

Compound 1b

Evidence for the major shape of the six-membered ring of **1b** were extracted from the analysis of the vicinal $^3J_{HH}$ coupling constants (Table 1), measured with and without ^{19}F-decoupling conditions (Figures S4 and S5 in the Supporting Information). As expected, very large $^3J_{H2H3}$ and $^3J_{H3H4}$ values were observed in water solution, thus demonstrating that it adopts a very major

Scheme 1. Reagents and conditions: i) bis(4-methoxyphenyl) disulfide (1.5 equiv), *n*Bu₃P, DMF, RT, overnight, 96%; ii) a) *m*CPBA (1.1 equiv), CH₂Cl₂, −20 °C to RT, overnight, 99%; b) DAST (5 equiv), CH₂Cl₂, 45 °C, 60 h, 96%; iii) Selectfluor (1.25 equiv), DAST (0.18 equiv), CH₃CN, RT, 45 min; then anhydrous DIPEA (1.5 equiv), RT, 45 min, 60%; iv) *m*CPBA (1.05 equiv), CH₂Cl₂, −20 °C to RT, overnight, 77%; v) Bn₃N (3 equiv) Ph₂O, 190 °C, 100 h, 36%; vi) a) I₂, PPh₃, imidazole, b) NaH, DMF, RT, 12 h, 82%; vii) O₃, Me₂S, −78 °C; viii) CBr₂F₂, HMPT, −15 to 45 °C, 3 h; ix) TIBAL (10 equiv), toluene, 50 °C, 30 min, 61%; x) Dess–Martin periodinane (3.7 equiv), CH₂Cl₂, RT, 2.5 h; xi) [(isopropoxy-dimethylsilyl)methyl]magnesium chloride, 4 Å MS, THF, 0 °C, 1 h; xii) TBAF (4 equiv), KHCO₃ (8 equiv), H₂O₂ (30 equiv), THF/MeOH (1:1, v/v), RT, 45 min, 57% over three steps; xiii) H₂, 10% Pd/C, MeOH, RT, 15 h, quant.

Table 1. $^3J_{HH}$ and $^nJ_{HF}$ coupling constants for **1a**, **1b** and **2** [Hz] in D_2O solution at 300 K and 500 MHz.[a]

Molecule	$^3J_{H1H2}$	$^3J_{H2H3}$	$^3J_{H3H4}$	$^3J_{H4H5}$	$^2J_{H6H6'}$	$^3J_{H1Fax}$	$^3J_{H1Feq}$	J_{H2Fax}	J_{H4Fax}	J_{H6Fax}	$^4J_{H6'Feq}$	$^2J_{FeqFax}$
1a	4.1	9.0	9.5	–	12.5	3.8[b]	7.3[b]	3.3	2.1	<1	2.8	270.0
1b	3.6	10.0	10.0	–	12.5	1.7	3.7	2.5	3.4	1.2	–	278.0
2	3.3	5.5	5.5	4.3	11.5	2.0	9.0	2.8	2.8	n.a.	–	270.0
Glc	3.8	9.8	9.1	10.1	12.3	–	–	–	–	–	–	–
Ido	1.7	4.1	4.6	2.5	–	–	–	–	–	–	–	–

[a] The observed values are in agreement with those expected for a very predominant $^4C_1$ conformation for **1a** and **1b** isomers, while intermediate values for **2** are observed. The experimental J coupling values for natural compounds are also provided. [b] Estimated from the corresponding ^1H NMR spectroscopic signals.

Table 2. ^1H and ^{19}F NMR spectroscopic chemical shifts for **1a**, **1b** and **2** [Hz] in D_2O solution at 300 K and 500 MHz.[a]

Molecule	δH1	δH2	δH3	δH4	δH5	δH6	δH6'	δFax	δFeq	δOMe
1a	3.82	3.64	3.60	3.50	–	3.89	3.96	−109.10	−119.40	3.48
1b	3.75	3.54	3.72	3.42	–	3.66	3.76	−110.20	−119.40	3.47
2	3.80	3.90	3.92	3.55	2.58	4.00	3.96	−98.70	−110.0	3.56
Glc	4.79	3.54	3.65	3.38	3.63	3.85	3.74	–	–	3.50
Ido	4.69	3.53	3.73	3.75	4.09	3.79	3.82	–	–	3.45

[a] Experimental chemical shift data for methyl-β-L-idopyranoside and methyl-α-D-glucopyranoside are also provided.

$^4C_1$ chair conformation. No significant variations of chemical shifts and coupling constants were appreciated upon decreasing the temperature (Figure S7 in the Supporting Information) from 298 down to 248 K (adding 20% of deuterated methanol). Similar couplings were observed for **1b** in [D_6]DMSO solution. Intermediate values for the $^3J_{H,OH}$ coupling constants were observed, ranging between 5.0 and 6.6 Hz (Table 3). Temperature coefficient factors were also of medium size for all the hydroxyl groups, between 4.9 and 7.0 ppb$^{\circ-1}$ (Table 4). These facts suggest that no particular orientations of the hydroxyl

Table 3. Observed $^3J_{H,OH}$ coupling constants [Hz] in DMSO solution at 300 K and 500 MHz.

	Coupling constants [Hz]				
	$^3J_{H4,OH4}$	$^3J_{H2,OH2}$	$^3J_{H3,OH3}$	$^3J_{H6',OH6}$	$^3J_{H6,OH6}$
1a	5.5	4.1	5.6	4.6	7.2
1b	6.1	5.0	6.6	5.9	5.9

Table 4. Temperature coefficients measured for the different hydroxyl groups of **1a** and **1b**, from the analysis of the ^1H NMR spectra recorded in DMSO between 298 and 343 K.[a]

	$\Delta\delta/\Delta T$ [ppb K^{-1}]						
	Fax	Feq	OH4	OH2	OH3	OH6	OH5
1a	8.4	17.2	6.9	6.5	6.5	5.1	4.6
1b	18	20	6.2	7.0	7.0	5.7	4.9

[a] The temperature coefficients of the fluorine atoms were deduced in D_2O using the same temperature range.

groups are favoured. No strong intramolecular hydrogen-bond between the hydroxyl moieties is present in [D_6]DMSO. Obviously, the presence of competing water molecules in the D_2O solution further precludes this possibility. Through-space coupling constants between the axial fluorine atom with H2, H4 and H6 were also deduced. Indeed, these couplings were also supported by heteronuclear ^1H–^{19}F NOEs between the corresponding atom pairs in the HOESY spectra (Figure S6 in the Supporting Information). No significant features were observed in the ^{19}F NMR spectra of **1b** acquired at low temperature (Figure S3 in the Supporting Information). Therefore, all the NMR parameters and observations were in agreement with the existence of a $^4C_1$ chair conformation, with no particular additional experimental observations worth mentioning.

Compound 1a (ido-like, difluoro, C5 is quaternary)

The ^{19}F NMR spectrum of **1a** was drastically different to that of **1b** (Figure 3) at room temperature. Strikingly, the signal of the axial fluorine sharpened in a noticeable manner upon decreasing the temperature down to 238 K (using 20% of methanol, Figure 4) or increasing it at 333 K. This fact suggests the exis-
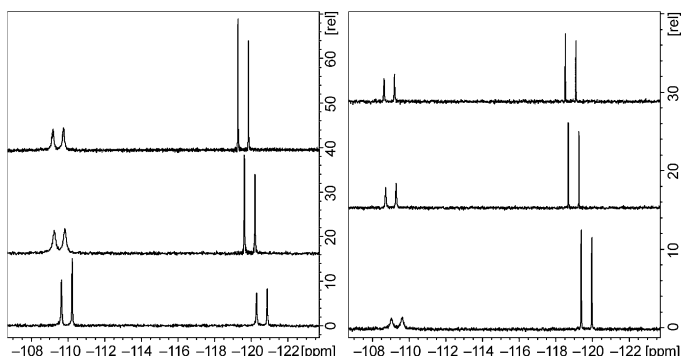

Figure 4. From bottom to top. ^{19}F NMR (470 MHz) spectra of **1a** at 238, 273 and 298 K (left), in D_2O in presence of 20% of methanol and at 283, 323 and 333 K (right) in D_2O.

tence of a dynamic process, which especially affects the transverse relaxation features of F_{ax}.

Curiously, the $^3J_{H2H3}$ and $^3J_{H3H4}$ coupling constant values (Table 1) were also relatively large in water solution, which suggests that a major $^4C_1$ chair conformation indeed exists at room temperature (see below, in the Discussion). As for **1b**, similar couplings were observed in [D_6]DMSO solution, together with medium-sized values (between 4.1 and 7.2 Hz) for the $^3J_{H,OH}$ couplings constants, (Table 3), and a narrow range of temperature coefficients (between 4.6 and 6.9 ppb$^{\circ-1}$) for the hydroxyl groups, (Table 4) which suggests the presence of conformational averaging around the corresponding C–O bonds. Again, there is no strong intramolecular hydrogen bond between the hydroxyl moieties in the employed solvents, in con-

trast with the observations for protected fluorine-containing carbohydrates in non-polar solvents.[40] Long-range coupling constants could also be detected, from the inspection of the ^1H NMR spectrum, between the axial fluorine with H2 (medium), H4 (small) and H6′ (2.8 Hz). Again, the corresponding heteronuclear $^1H/^{19}F$ NOEs were observed for the $^1H/^{19}F$ pairs in the HOESY spectrum (Figures S10 and S11 in the Supporting Information). Indeed, additional information on the geometry of 1 a was obtained through the careful analysis of the $^1H/^1H$ homo- and $^1H/^{19}F$ heteronuclear NOE experiments (Figure 5 and Table S2 in the Supporting Information). Two key cross-peaks were observed for 1 a. There is a medium-size H3/H6 NOE, and a weak H3/H6′ one. Moreover, a clear heteronuclear H6/F_{eq} NOE was also observed, while the corresponding H6′/Feq NOE was rather weak. The vicinal couplings between the two H6 protons in 1 a and the corresponding OH6 were somehow different (2.6 Hz of difference). These findings are only compatible with the existence of conformational averaging in solution. The HOESY spectrum in DMSO (Figure S13 in the Supporting Information) showed the Fax/OH5 NOE, be-

sides those observed in D_2O solution. No NOEs with other hydroxyl groups were observed for the two ^{19}F atoms.

The observed data suggests that the differences in the ^{19}F NMR spectra between 1 b and 1 a derive from a different dynamic behaviour of both molecules. Nevertheless, still for 1 a, the relatively large $^3J_{H2H3}$ and $^3J_{H3H4}$ coupling constant values point out the existence of a major $^4C_1$ conformation for the six-membered ring. Moreover, the simultaneous spatial proximity between the H3/H6 and F_{eq}/H6 pairs, together with the through-space coupling constant between F_{ax} and H6′ strongly suggests the existence of two orientations around C5—C6, as schematized in Figure 5. Moreover, in order to justify the weak H6′/F_{eq} NOE, a minor contribution of the $^2S_{5a}$ conformer has to be also considered (see also below).

Low-temperature NMR experiments in water solution (with 20% methanol) provided additional information on the nature of the conformational equilibrium. It was observed that H1 shifted downfield upon decreasing temperature, while H2, H3 and H4 were shifted upfield (Figure S14 in the Supporting Information). Strikingly, H6 and H6′ interchanged chemical shifts
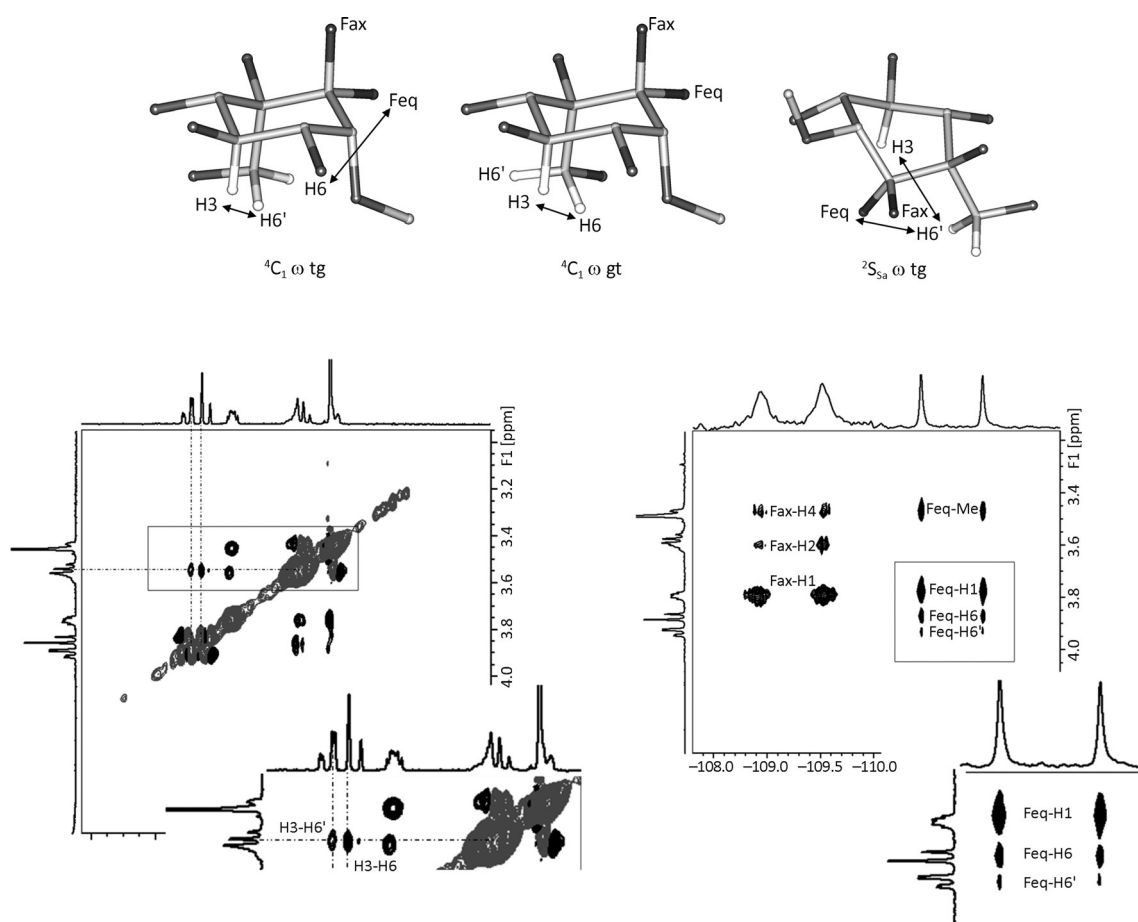

Figure 5. Top panel, schematic representation of the three major conformations present for 1 a. The arrows highlight the existence of NOE cross-peaks. No unique geometry is able to completely explain the NOE data, but a combination of all the represented structures does it. ω is defined by (O6-C6-C5-C5a) and (O6-C6-C5-C4) torsion angles. The $^4C_1$ gt conformer also justifies the H6′/Fax long-range coupling constant given its relative W-like arrangement between the two coupled nuclei. Left, 2D NOESY spectra (700 ms mixing time) of compound 1 a at 600 MHz and 298 K in D_2O. Key NOEs are highlighted in the strip taken at H3 frequency. No other NOEs are observed above the noise level. Right, ^1H-^{19}F HOESY spectrum (470/500 MHz Bruker spectrometer) of 1 a in D_2O in the presence of 20% methanol (800 ms mixing time). The strips taken at frequency of equatorial fluorine are highlighted.

during the cooling process. As mentioned above, the axial ^{19}F NMR signal became sharper at low temperature and no additional ^{19}F signals were evident.

Compound 2

The ^{19}F NMR spectrum of **2** displayed two broad ^{19}F NMR spectroscopic signals (Figure 6) at room temperature. Interestingly,
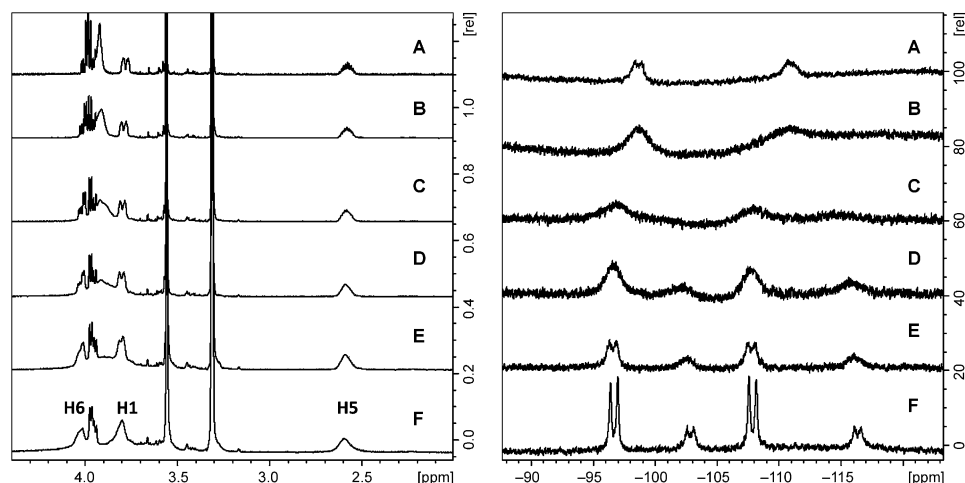

Figure 6. Variable temperature ^1H NMR (left) and decoupled ^{19}F-{^1H} NMR spectrum (right) of **2** in D_2O (with 20% methanol) at 500 (^1H) or 470 (^{19}F) MHz. From top to bottom: A) 318, B) 298 K, C) 283 K, D) 273 K, E) 263 K, F) 253 K. Notice that the chemical shifts of the ^1H NMR spectroscopic signals do not show major shifts with temperature.

the signals sharpened in a noticeable manner upon decreasing the temperature and two new clear ^{19}F NMR spectroscopic signals appeared at 253 K (using a 20% of methanol, Figure 6). The conformational equilibrium is slow in the ^{19}F NMR chemical shift scale at this temperature. Using the observed coalescence temperature between 283 and 298 K and the estimated chemical shift difference of the two set of fluorine signals at 253 K, the energy barrier was calculated to be approximately 11.8 ± 0.4 kcal mol^{-1}.[41] The relative populations of the two signals were 70:30, which indicated that the free-energy difference was of only approximately 0.4 kcal mol^{-1}.

Because of the severe proton overlapping, the *J* coupling constants were extracted from spectral simulation (Figure S16 in the Supporting Information). The $^3J_{H2H3}$ and $^3J_{H3H4}$ (Table 1) values were intermediate (ca. 5.5 Hz for both) in solution, which suggests the presence of a conformational equilibrium, as shown by the two sets of ^{19}F signals at 253 K. In contrast to the observations for **1a**, in this case, it was observed that none of the ^1H NMR spectroscopic signals were significantly shifted at low temperature. As will be described below in the discussion, this behaviour also contains key conformational information.

Computational methods

The molecular modelling protocol described in the Experimental Section was adopted for structure assessment, providing

different possible conformers for the molecules discussed here (Figure 7).

For the Glc-configurated **1b**, the theoretical calculations well predicted the $^4C_1$ as unique possible conformer. The other two local minima, $^1C_4$ and $^1S_3$, displayed much larger relative free energy, about 11.0 and 8.0 kcal mol^{-1}, respectively. For this system, the transition-state structures were also deduced to build the potential energy surface. The activation energies were estimated as approximately 15.0 kcal mol^{-1} for the ^3E envelope and 13.5 kcal mol^{-1} for the $^{5a}H_5$ half-chair shapes.

For **2**, the alternative $^1C_4$ chair was predicted as the global minimum, with the $^4C_1$ chair destabilized in approximately 1.7 kcal mol^{-1}. In this case, the equatorial orientation of the two bulky groups is probably the impetus for the calculated energy values. In this case, the $^2S_{5a}$ conformer displayed the less favourable energy value.

For **1a**, the $^1C_4$ form was strongly destabilized with respect to the global minimum, the $^4C_1$ conformer. The presence of several 1,3-diaxially oriented

| Relative Energy (kcal mol^{-1}) | 0.0 | 4.0 | 10.0 |

1a methyl-β-L-idopyranoside

| Relative Energy (kcal mol^{-1}) | 0.0 | 8.0 | 11.0 |

1b methyl-α-D-glucopyranoside

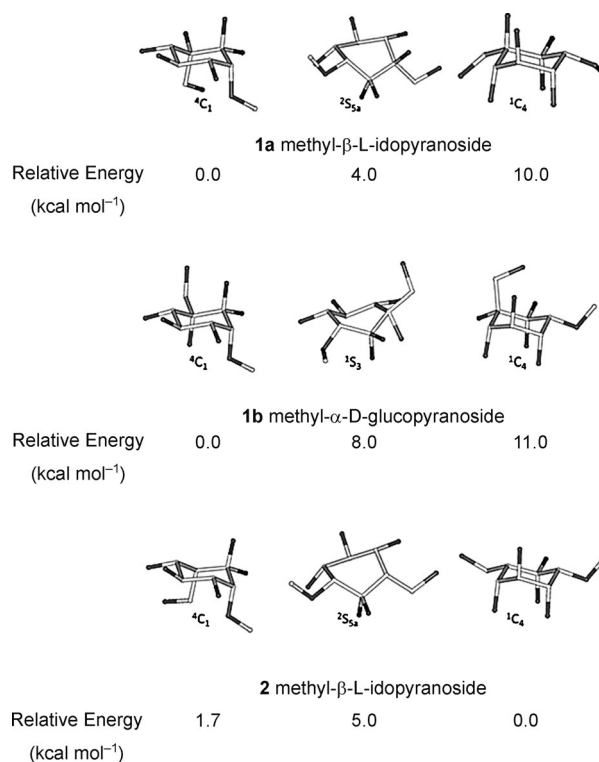| Relative Energy (kcal mol^{-1}) | 1.7 | 5.0 | 0.0 |

2 methyl-β-L-idopyranoside

Figure 7. Ball and stick representation and relative steric energy values of the major conformers of **1a**, **1b** and **2**, according to DFT calculations (see also the Supporting Information).

groups provides the structural basis for these predictions. The $^2S_{5a}$ skew boat displays most of the bulky groups in pseudo-equatorial orientations, resulting in a relative low destabilizing energy value (4.0 kcal mol^{-1}).

The conformational behaviour of idose rings and derivatives thereof has been a matter of investigation for years.[22,42–45] It is well known that for L-idopyranoses, the theoretically more favourable $^1C_4$ chair displays three axially oriented hydroxyl groups, with the corresponding steric consequences. The alternative $^4C_1$ chair places the bulky hydroxymethyl group at the axial orientation, with the corresponding collapse. Therefore, alternative skew-boat conformers are also present in the conformational equilibrium, depending on the hydroxyl substitution, chemical environment, and solvent.[46–48] Therefore, the description of the conformational flexibility of these rings in terms of thermodynamic parameters as activation free energy, and entropic and enthalpy contributions to the Gibbs free energy difference represents a challenge to the experimental study. Such a description implies access to a detailed and accurate proton-proton coupling constant analysis, which is hampered by signal broadening and or overlapping. In fact, the situation becomes even more arduous, and most of the times inaccessible, in cases of fast and medium conformational equilibria in the NMR chemical shift timescale, especially when it involves entropically favoured isoforms, such as skew boat conformers, which is often the case for idose ring derivatives.

As mentioned above, for ido-like sugars, flexibility is intrinsically related to biological activity. The sulfated L-iduronic rings represent the paradigmatic example of how plasticity modulates the interaction with biological receptors. From the chemical perspective, these molecular recognition processes are the consequence of the balance between enthalpy and entropy factors and solvation/desolvation effects. In this context, since conformational entropy becomes an issue, it is essential to consider that the conformational entropy of chair and skew boat conformers is intrinsically different. Chair conformers are defined in well-characterized potential energy wells, while the conformational entropy of skew boat conformers is larger, due to the low-energy cost geometry interconversions that conduct to basically the same conformer. The energy well for skew boat conformers is much wider than that for the chairs.

Under these premises, the obtained results can now be accounted for in a satisfactory manner. Compound **1b** (Glc-like) displays a unique $^4C_1$ chair conformer with a very well defined geometry, as in the natural compound. Similarly to the natural Ido-like molecule, compound **2**, displays significant conformational distortions. There is a clear-cut behaviour for compound **2**. ^{19}F-based variable temperature experiments demonstrate the existence of a conformational equilibrium between two forms with an approximately 70:30 population distribution. The observed coupling constants are in fact in agreement with a 70:30 distribution between the canonical $^4C_1$ (minor) and $^1C_4$ (major) chair forms (Table S4 in the Supporting Information). No changes in either chemical shifts or coupling constants are observed with temperature, which indicates that the conformational distribution is temperature-independent. Therefore, the conformational entropy of the contributing geometries is

similar, as expected for the two alternative $^4C_1$ and $^1C_4$-chair conformers. The free-energy difference between the two forms is approximately 0.4 kcal mol^{-1}, favouring the $^1C_4$ chair in the same trend as the energy differences estimated by the calculations. The energy barrier for interconversion is relatively low (ca. 11.8 kcal mol^{-1}), extremely difficult to access by variable temperature ^{1}H NMR spectroscopic experiments in water solution. The use of ^{19}F NMR spectroscopy has permitted access to this value, due to the wide accessible chemical shift range. Indeed, computational chemistry calculations using ab initio methods (DFT (B3LYP) in vacuum with the different basis sets: 6-31+ +G, for the $^4C_1$ and $^1C_4$ geometries; 6-31+ +G + freq, for $^2S_{5a}$; and 6-31+ +GTS + freq, for ^3E and $^{5a}H_5$), provided energy values fairly similar to those experimentally detected (12.5 kcal mol^{-1} for ^3E and 13.0 for $^{5a}H_5$).

In contrast, compound **1a** shows a unique conformational behaviour. The chemical shift and coupling constant values drastically changed upon temperature variation (Figure S14 in the Supporting Information) indicating that its conformational distributions depend on the temperature. This observation strongly suggests that the conformational entropy of the contributing geometries is different. At low temperature, the enthalpy-favoured conformer should be predominant, since the entropy contribution to free energy will be largely attenuated ($\Delta G = \Delta H - T\Delta S$). Fittingly, H2, H3, and H4 shift upfield more than $\delta = 0.1$ ppm upon decreasing temperature. Concomitantly, H1 shifted downfield. This fact provides evidence that, at low temperature, the predominant conformer of **1a** displays H2, H3 and H4 in axial orientation, while H1 shows an equatorial arrangement. Therefore, the major and enthalpy-favoured conformer is the $^4C_1$ chair. The other participating conformer should display a skew boat geometry since its contribution to the conformational equilibrium strongly decreases at low temperature. Computational chemistry calculations found the $^2S_{5a}$ conformer as the most stable skew boat form, with a relative energy of about 4.0 kcal mol^{-1} with respect to the $^4C_1$ chair. The $^1C_4$ form was strongly destabilized, by more than 10 kcal mol^{-1}. In fact, for the $^2S_{5a}$ conformer, H2, H3 and H4 display a quasi-axial orientation, providing large $^3J_{H2H3}$ and $^3J_{H3H4}$ couplings.

Since these observed $^3J_{H2H3}$ and $^3J_{H3H4}$ couplings at room temperature for both molecules were already rather large (above 9 Hz), the contribution of the skew boat conformers would have been clearly neglected from the inspection of the ^{1}H and ^{13}C NMR spectra, unless the ^{19}F NMR spectra would not have shown dramatically broad signals.

Interestingly, the conformational behaviour of these ^{19}F-containing glycomimetics remarkably resembles the intrinsic flexibility of the natural Ido-configurated sugars (Table S5 in the Supporting Information). Although this fact might not completely surprising, as a matter of fact, regular Ido-like carbasugars,[49] with a CH_2 group mimicking the endocyclic oxygen atom, did not show any conformational plasticity (Table S5 in the Supporting Information). In contrast, the molecules presented herein, with CF_2 moieties resembling the endocyclic oxygen atom show important conformational plasticity. The dynamic process has been quantified in terms of energy barri-

ers and free-energy differences. The destabilizing energies for the $^4C_1$ conformer in **2** is 0.4 kcal mol^{-1} above that for the $^1C_4$ chair. However, when C5 is modified (as in **1a**, with one additional OH substituent), there is a participation of skew boat conformers, while the proportion of the $^1C_4$ conformer is strongly diminished. The OH3 group displays an equatorial orientation in the $^4C_1$ and $^2S_{5a}$ geometries, minimizing the influence of steric conflicts with the additional OH5. However, it would adopt an axial disposition in the $^1C_4$ form, provoking important additional steric clashes. For the Glc-like molecules, the conformational behaviour of the CF$_2$ analogue also mimics that of natural glucopyranosides. Therefore, these glycomimetics can behave as conformational bioisosteres.

Conclusions

A new generation of fluorine-containing glycomimetics is presented. The importance of introducing fluorine atoms in these glycomimetics is also highlighted. First, only the use of ^{19}F NMR spectroscopic experiments has permitted the detection of a dynamic process of paramount significance that would have been otherwise remained unobserved. Additionally, only in the presence of fluorine atoms at C5a, the Ido-like six-membered ring recovers its required flexibility, absent in regular CH$_2$-Ido-carbasugars,[38] while the presence of a bulky substituent at position C5 strongly reduces the ring flexibility and introduces important steric clashes. A recent report from our group[20] has shown that the CF$_2$ moiety partially recovers the *exo*-anomeric effect typical of oligosaccharides, thus resembling the conformational behaviour of glycans around the glycosidic linkage. Herein, we also demonstrate that the presence of the fluorine in the ring additionally restores the plasticity of Ido-like six-membered rings.

Thus, the combination of NMR spectroscopic experiments and computational methods has permitted the demonstration that these idose-like analogues resemble the conformational plasticity of the natural parent molecules that is anticipated to be required for the key molecular recognition process and ultimately for biological activity.

Experimental Section

NMR Spectroscopy

^{19}F NMR spectroscopic experiments were performed 470 MHz with a Bruker AVANCE spectrometer equipped with the proper fluorine probe SEF, at 298 K unless otherwise stated while low temperature experiments were done with Bruker DRX 500 MHz equipped with BBOF plus probe. ^{1}H NMR spectroscopic experiments were performed at 600 and 700 MHz with a Bruker AVANCE spectrometer equipped with TXI probe. Experiments were performed in D$_2$O, [D$_6$]DMSO and in D$_2$O in the presence of 20% methanol for low temperature analysis. The concentration employed was 2 mM for all the discussed molecules. In addition to standard 1D ^{1}H NMR spectra, COSY, TOCSY, NOESY and HOESY (800 ms mixing time) and ^{1}H/^{13}C HSQC experiments based on the standard BRUKER sequences were also acquired, in order to assign the resonance of all NMR spectroscopic signals. Because of the severe proton overlapping,

the *J* coupling constants were extracted from spectral simulation using MestreNova software. The method of determining activation energy parameters is through the estimation of the coalescence temperature and chemical shift difference for each of the fluorine signals measured in the spectrum at lower temperature (253 K) giving 2900 Hz for low-field signals and 4010 Hz for higher field signals.[41] The exchange rate for both fluorine signals can be now estimated by applying Equation (1):

$$kc = \frac{\pi \Delta v}{\sqrt{2}} \tag{1}$$

After observing the fluorine NMR spectra at different temperatures (Figure 6), it was possible to enclose the activation energy barrier between the limiting values calculated for 283 and 298 K by applying the Eyring equation [see Eq. (2)]:

$$\Delta G^{\neq} = RT_c \left[\ln\left(\frac{K_B T_c}{h}\right) - \ln(kc) \right] \tag{2}$$

in which *R* is the gas constant, T_c the coalescence temperature, K_B the Boltzmann constant, *h* the Planck constant, and *kc* the determined exchange rate. With this above equation, the activation energy barrier relative to the low-field signal lies between the limiting values of 11.6 kcal mol^{-1} at 283 K and 12.2 kcal mol^{-1} at 298 K, giving an average value of 11.9 kcal mol^{-1} at the estimated coalescence temperature of 290 K, while for the high-field signal it lies between 11.4 and 12.0 kcal mol^{-1} with an average value of 11.7 kcal mol^{-1} at 290 K. The final estimation for the activation energy is $\Delta G^{\neq} = 11.8$ kcal mol^{-1} ± 0.4.

Computational methods

A conformational search on these molecules **1a**, **1b** and **2** was performed by using Macromodel at the Maestro suite of programs, with the MM3* force field. Different local minima conformers were chosen within a conservative 20 kcal mol^{-1} threshold from the global minimum. Their expected coupling constant values and proton–proton distances (related to NOEs) were estimated from the corresponding structures using Maestro. The transition-state geometries for the interconversion process were chosen based on the well known Cremer–Pople sphere conformational routes. Then, the MM3*-optimized structures were used as starting conformations for additional ab initio calculations. Thus, DFT geometry optimizations were performed with the Gaussian 03 program using the hybrid B3LYP functional and the 6–31++G(d,p) basis set followed by vibrational frequency analysis. This protocol allowed assessing whether the optimized structures were true energy minima, transition states, or saddle points. For the transition-states structures, the final geometry optimization was achieved by applying the TS Berny algorithm. In all cases, the presence of solvent was accounted for by the integral equation formalism polarizable continuum model (IEFPCM). The NMR isotropic shielding constants were calculated using the standard Gauge Independent Atomic Orbital (GIAO) approach. The experimental and calculated NMR coupling constants were then compared.

Acknowledgements

[1] D. Solís, N. V. Bovin, A. P. Davis, J. Jiménez-Barbero, A. Romero, R. Roy, K. Smetana, Jr., H.-J. Gabius, *Biochim. Biophys. Acta* **2015**, *1850*, 186–235.

[2] H.-J. Gabius, S. André, J. Jiménez-Barbero, A. Romero, D. Solís, *Trends Biochem. Sci.* **2011**, *36*, 298–313.

[3] S. A. W. Gruner, E. Locardi, E. Lohof, H. Kessler, *Chem. Rev.* **2002**, *102*, 491–514.

[4] Q. H. Fan, K. A. Claunch, S. Striegler, *J. Med. Chem.* **2014**, *57*, 8999–9009.

[5] A. Ardá, P. Blasco, D. Varón Silva, V. Schubert, S. André, M. Bruix, F. J. Cañada, Jr., H.-J. Gabius, C. Unverzagt J. Jiménez-Barbero, *J. Am. Chem. Soc.* **2013**, *135*, 2667–2675.

[6] L. Unione, S. Galante, D. Díaz, F. J. Cañada, J. Jiménez-Barbero, *Med. Chem. Commun.* **2014**, *5*, 1280–1289.

[7] M. C. Fernández-Alonso, D. Díaz, M. A. Berbis, F. Marcelo, F. J. Cañada, J. Jiménez-Barbero, *Curr. Protein Pept. Sci.* **2012**, *13*, 816–830.

[8] A. Canales, A. Mallagaray, M. A. Berbís, A. Navarro-Vázquez, G. Domínguez, F. J. Cañada, S. André, Jr., H.-J. Gabius, J. Pérez-Castells, J. Jiménez-Barbero, *J. Am. Chem. Soc.* **2014**, *136*, 8011–8017.

[9] A. García-Herrero, E. Montero, J. L. Muñoz, J. F. Espinosa, A. Vián, J. L. García, J. L. Asensio, F. J. Cañada, J. Jiménez-Barbero, *J. Am. Chem. Soc.* **2002**, *124*, 4804–4810.

[10] P. Vidal, V. Roldós, M. C. Fernández-Alonso, B. Vauzeilles, Y. Blériot, F. J. Cañada, S. André, Jr., H.-J. Gabius, J. Jiménez-Barbero, J. F. Espinosa, S. Martín-Santamaría, *Chem. Eur. J.* **2013**, *19*, 14581–14590.

[11] M. Risseeuw, M. Overhand, G. W. Fleet, M. I. Simone, *Amino Acids* **2013**, *45*, 613–689.

[12] J. Jiménez-Barbero, J. F. Espinosa, J. L. Asensio, F. J. Cañada, A. Poveda, *Adv. Carbohydr. Chem. Biochem.* **2000**, *56*, 235–284.

[13] E. Montero, A. García-Herrero, J. L. Asensio, K. Hirai, S. Ogawa, F. Santoyo-González, F. J. Cañada, J. Jiménez-Barbero, *Eur. J. Org. Chem.* **2000**, 1945–1952.

[14] B. López-Méndez, C. Jia, Y. Zhang, P. Sinaÿ, L.-H. Zhang, J. Jiménez-Barbero, M. Sollogoub, *Chem. Asian J.* **2008**, *3*, 51–58.

[15] A. Vulpetti, U. Hommel, G. Landrum, R. Lewis, C. Dalvit, *J. Am. Chem. Soc.* **2009**, *131*, 12949–12959.

[16] E. Leclerc, X. Pannecoucke, M. Ethève-Quelquejeu, M. Sollogoub, *Chem. Soc. Rev.* **2013**, *42*, 4270–4283.

[17] E. Prchalová, O. Stepánek, S. Smrcek, M. Kotora, *Future Med. Chem.* **2014**, *6*, 1201–1229.

[18] A. Deleuze, C. Menozzi, M. Sollogoub, P. Sinaÿ, *Angew. Chem. Int. Ed.* **2004**, *43*, 6680–6683; *Angew. Chem.* **2004**, *116*, 6848–6851.

[19] J. Sardinha, S. Guieu, A. Deleuze, M. C. Fernández-Alonso, A. P. Rauter, P. Sinaÿ, J. Marrot, J. Jiménez-Barbero, M. Sollogoub, *Carbohydr. Res.* **2007**, *342*, 1689–1703.

[20] B. Xu, L. Unione, J. Sardinha, S. Wu, M. Ethève-Quelquejeu, A. P. Rauter, Y. Blériot, Y. Zhang, S. Martín-Santamaría, D. Díaz, J. Jiménez-Barbero, M. Sollogoub, *Angew. Chem. Int. Ed.* **2014**, *53*, 9597–9602; *Angew. Chem.* **2014**, *126*, 9751–9756.

[21] C. Dalvit, A. Vulpetti, *ChemMedChem* **2012**, *7*, 262–272.

[22] B. Casu, J. Choay, D. R. Ferro, G. Gatti, J.-C. Jacquinet, M. Petitou, A. Provasoli, M. Ragazzi, P. Sinaÿ, G. Torri, *Nature* **1986**, *322*, 215–216.

[23] J. Turnbull, A. Powell, S. Guimond, *Trends Cell Biol.* **2001**, *11*, 75–82.

[24] W. Li, D. J. Johnson, C. T. Esmon, J. A. Huntington, *Nat. Struct. Mol. Biol.* **2004**, *11*, 857–862.

[25] A. Canales, R. Lozano, B. López-Méndez, J. Angulo, R. Ojeda, P. M. Nieto, M. Martín-Lomas, G. Giménez-Gallego, J. Jiménez-Barbero, *FEBS J.* **2006**, *273*, 4716–4727.

[26] S. K. Das, J.-M. Mallet, J. Esnault, P.-A. Driguez, P. Duchaussoy, P. Sizun, J.-P. Hérault, J.-M. Herbert, M. Petitou, P. Sinaÿ, *Angew. Chem. Int. Ed.* **2001**, *40*, 1670–1673; *Angew. Chem.* **2001**, *113*, 1723–1726.

[27] J. Rönnols, S. Manner, A. Siegbahn, U. Ellervik, G. Widmalm, *Org. Biomol. Chem.* **2013**, *11*, 5465–5472.

[28] J. Rönnols, S. Manner, U. Ellervik, G. Widmalm, *Org. Biomol. Chem.* **2014**, *12*, 8031–8035.

[29] E. T. Jarvi, J. R. McCarthy, S. Mehdi, D. P. Matthews, M. L. Edwards, N. J. Prakash, T. L. Bowlin, P. S. Sunkara, *J. Med. Chem.* **1991**, *34*, 647–656.

[30] H. Paulsen, M. Paal, *Carbohydr. Res.* **1983**, *113*, 203–218.

[31] D. Semeria, M. Philippe, J.-M. Delaumeny, A.-M. Sepulchre, S. D. Gero, *Synthesis* **1983**, 710–713.

[32] G.-N. Wang, G. Reinkensmeier, S.-W. Zhang, J. Zhou, L.-R. Zhang, L.-H. Zhang, T. D. Butters, X.-S. Ye, *J. Med. Chem.* **2009**, *52*, 3146–3149.

[33] S. K. Das, J.-M. Mallet, P. Sinaÿ, *Angew. Chem. Int. Ed. Engl.* **1997**, *36*, 493–496; *Angew. Chem.* **1997**, *109*, 513–516.

[34] M. Sollogoub, J.-M. Mallet, P. Sinaÿ, *Tetrahedron Lett.* **1998**, *39*, 3471–3472.

[35] M. Sollogoub, A. J. Pearce, A. Hérault, P. Sinaÿ, *Tetrahedron: Asymmetry* **2000**, *11*, 283–294.

[36] A. J. Pearce, M. Sollogoub, J.-M. Mallet, P. Sinaÿ, *Eur. J. Org. Chem.* **1999**, 2103–2117.

[37] M. Sollogoub, J.-M. Mallet, P. Sinaÿ, *Angew. Chem. Int. Ed.* **2000**, *39*, 362–364; *Angew. Chem.* **2000**, *112*, 370–372.

[38] B. M. Sattelle, B. Bose-Basu, M. Tessier, R. J. Woods, A. S. Serianni, A. Almond, *J. Phys. Chem. B* **2012**, *116*, 6380–6386.

[39] M. U. Roslund, P. Tähtinen, M. Niemitz, R. Sjöholm, *Carbohydr. Res.* **2008**, *343*, 101–112.

[40] G. T. Giuffredi, V. Gouverneur, B. Bernet, *Angew. Chem. Int. Ed.* **2013**, *52*, 10524–10528; *Angew. Chem.* **2013**, *125*, 10718–10722.

[41] J. Von Sandström, *Dynamic NMR Spectroscopy*, Academic Press, London **1982**.

[42] J. Rönnols, S. Manner, U. Ellervik, G. Widmalm, *Org. Biomol. Chem.* **2014**, *12*, 8031–8035.

[43] J. R. Snyder, A. S. Serianni, *J. Org. Chem.* **1986**, *51*, 2694–2702.

[44] M. B. Sattelle, U. S. Hansen, J. Gardiner, A. Almond, *J. Am. Chem. Soc.* **2010**, *132*, 13132–13134.

[45] A. Canales, J. Angulo, R. Ojeda, M. Bruix, R. Lozano, G. Giménez-Gallego, M. Martín-Lomas, P. M. Nieto, J. Jiménez-Barbero, *J. Am. Chem. Soc.* **2005**, *127*, 5778–5779.

[46] A. Ardèvol, X. Biarnés, A. Planas, C. Rovira, *J. Am. Chem. Soc.* **2010**, *132*, 16058–16065.

[47] J. Angulo, P. M. Nieto, M. Martín-Lomas, *Chem. Commun. (Camb)* **2003**, 1512–1513.

[48] X. Biarnés, A. Ardèvol, A. Planas, C. Rovira, A. Laio, M. Parrinello, *J. Am. Chem. Soc.* **2007**, *129*, 10686–10693.

[49] E. Säwén, M. U. Roslund, I. Cumpstey, G. Widmalm, *Carbohydr. Res.* **2010**, *345*, 984–993.